

3. CONCEPTUAL TRANSPORT MODEL

The migration of contaminants from the underground nuclear tests at Amchitka involve a complex system of physical and chemical processes. Some of these processes are poorly understood and are the subject of ongoing research conducted by the U.S. Department of Energy. For the analysis of Amchitka, many assumptions were made based on currently available data. A diagrammatic representation of the transport model source and processes considered is shown in Figure 3.1.

The contaminants considered consist of the radionuclides produced by Milrow, Long Shot, and Cannikin and the daughters created by radioactive decay. The nuclides are assumed to all be located within the cavity. Distribution upward through the chimney region was neglected. Sampling in the Cannikin post-test hole confirms that the bulk of radioactivity is contained within the cavity region (Claassen, 1978). In general, the primary effect of spreading the source nuclides through a larger volume is to disperse and dilute the mass, lowering concentrations.

Radionuclides are distributed according to their volatility among surface deposits and volume deposits in nuclear melt glass. Volatile and surface-deposited nuclides are assumed to migrate immediately after the nuclear test, neglecting the time of groundwater infill, when hydraulic gradients are directed toward the cavity. Nuclides within the glass are released according to glass dissolution rates calculated based on volcanic glass dissolution behavior and radionuclide melt glass characteristics. Early time cavity conditions and near-field properties affected by the nuclear tests were not considered in the analysis, presuming that the scale of transport considered here (thousands of meters), renders the calculations insensitive to the near-cavity environment. Residual heat from a test is considered in a sensitivity analysis.

Once released, the nuclides are subjected to retardation processes. Diffusion of contaminants from fractures into surrounding matrix blocks is also considered. Some radionuclides are retarded by reactions with aquifer materials. Retardation factors are calculated from a surface-based sorption

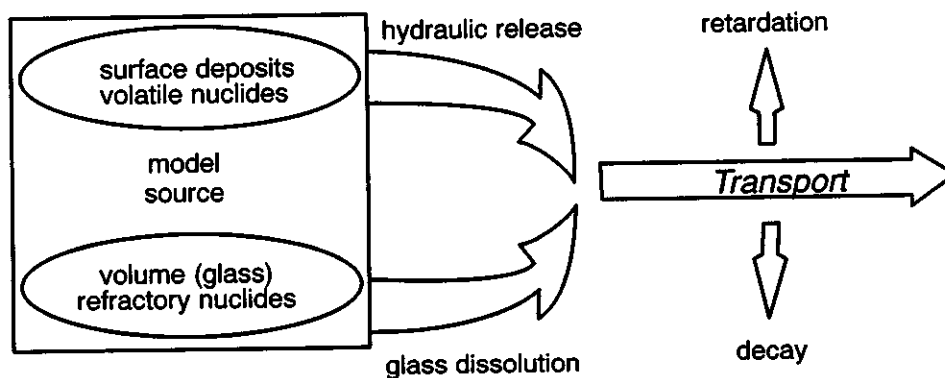


Figure 3.1. Flow chart of the transport model source and processes considered.

constant for the fractures, based on estimates of fracture aperture and distribution coefficients derived from batch experiments on Amchitka cores. Nuclides were grouped according to assumed general sorptive behavior and assigned the same retardation factor because radionuclide-specific data are not available for many of the contaminants in the Amchitka environment. The effect of colloidal particles on transport behavior was not modeled due to the lack of data to support such calculations and the observations from other sites that the mass actually transported by colloids would necessarily be exceedingly small.

The transport calculations are performed using a particle tracking method. An initial mass is released and its movement tracked through the model domain, with breakthrough at the ocean floor recorded. The mass breaking through is the input needed for a risk assessment model. The effect of radioactive decay was calculated in a post-processing mode. All of the contaminant masses used in the transport modeling are assigned a value of one. The results can then be scaled by the classified masses available in Goishi *et al.* (1995), or any unclassified estimates available.

3.1 Source Term and Release Parameters

3.1.1 Radionuclide Source Term

Contaminants from underground nuclear testing can be divided into two broad categories: radionuclides and non-radionuclides. Primary radionuclides can be attributed to three possible origins: 1) residual nuclear material that has not undergone a fission or a thermonuclear reaction, 2) direct products of the nuclear reactions (fission products and tritium), and 3) activation products induced by neutron capture in the immediate vicinity of the explosion (Borg *et al.*, 1976). In addition, radionuclide daughter products are produced by decay of many of the primary radionuclides.

The radionuclide source terms for Milrow, Long Shot, and Cannikin are included in an inventory prepared by Los Alamos and Lawrence Livermore national laboratories for nuclear tests conducted at non-NTS locations (Goishi *et al.*, 1995). This inventory represents the total radionuclide source term, given the following constraint. Radionuclides are excluded from the inventory if they are produced in such low amounts or decayed so rapidly that dissolving the total amount produced during the test into a volume of water equal to the volume of the cavity and allowing decay for 100 years resulted in an aqueous concentration less than one-tenth of the maximum permissible concentration (MPC) (Smith *et al.*, 1995). This effectively eliminates radionuclides with half-lives less than about ten years from the inventory.

A shorter list of radionuclides of significance for remedial investigations at the NTS is compiled considering the 56 radionuclides presented by Goishi *et al.* (1994) for the NTS, and eight additional radionuclides with half-lives less than ten years that had been encountered in samples of cavity fluids (Smith, 1997). This shorter list is based on the production of a radionuclide in a nuclear test, the relative mobility of the radionuclide determined from historical observations, and the health effects of the radionuclide relative to a total body or organ dose. The source term considered in this work is comprised of the radionuclides common to the Goishi *et al.* (1995) inventory list and the Smith (1997) list of significant radionuclides. Our source contains a total of 24 nuclides (several are

stable), including parents and daughters (Table 3.1). These radionuclides cover the gamut of release functions and retardation properties (discussed in following sections) and thus can be considered representative of the full radionuclide source term contained in Goishi *et al.* (1995).

Table 3.1. List of radionuclides considered for the source-term for Milrow, Long Shot, and Cannikin.

Radionuclide	Half-life, years	MPC, pCi/L
^3H	12.3	20,000
^{14}C	5730	2,000
^{36}Cl	3.01×10^5	700
^{85}Kr	10.73	NA
^{90}Sr	29.1	8
^{99}Tc	2.13×10^5	900
^{129}I	1.57×10^7	1
^{137}Cs	30.17	200
^{151}Sm	90	1,000
^{152}Eu	13.48	200
^{234}U	2.46×10^5	90
^{238}U	4.47×10^9	100
^{237}Np	2.14×10^6	5
^{239}Pu	2.41×10^4	8
^{240}Pu	6.56×10^3	8
$^{241}\text{Am}^*$	432.7	10
daughters:		
^{85}Rb	stable	
^{90}Y	7.3×10^{-3}	60
^{90}Zr	stable	
^{137}Ba	stable	
^{151}Eu	stable	
^{152}Gd	1×10^{14}	NA
^{236}U	2.3×10^7	90
^{237}Np	2.14×10^6	5

* initial ^{241}Pu will be decayed to ^{241}Am and added to its mass

The initial mass data for the radionuclides produced by the Amchitka tests remain classified (Goishi *et al.*, 1995) and cannot be presented in a public document. The transport calculations presented in this report are performed using a unit value for starting mass. The unit-mass-based transport analyses can be converted to true mass in a classified companion document, when the need arises.

3.1.1.1 Radioactivity Observed in Cannikin Cavity Water

Of the three tests, post-test sampling results are only available for Cannikin. The re-entry hole UA-1-P1 was completed 106 days after the test and subsequently logged, perforated, and sampled.

The detailed results of investigations in the hole are reported by Claassen (1978). Gamma logging identified high activity spikes in the region of the cavity, coincident with a large increase in temperature. The five perforated intervals span this cavity zone and above, with the uppermost perforation about 200 m above the cavity size estimated here. Sampling was only performed with thief samplers, plugging of perforations required surging, and significant borehole flow was observed, all requiring great care for interpreting the data. Data collected prior to July 1972 exhibit the impacts of condensed steam prior to cavity infill and are not interpreted by Claassen as being representative of saturated cavity conditions. Claassen points out that samples from the re-entry hole are probably not representative of bulk cavity water, but that they should be representative of the isotopes present, but at lower concentrations due to dilution and mixing.

As expected, elevated tritium concentrations are present in the samples (Figure 3.2). Very little alpha activity was observed in any of the samples. The few exceptions could be accounted for by natural alpha in the drilling fluids used in the hole. Three samples were analyzed specifically for ^{239}Pu , ^{240}Pu , ^{238}U , and ^{235}U . No plutonium was detected and the uranium-isotope ratio indicated natural uranium was present in all three. Comparing the gross beta/gamma results for other waters on the island with those from UA-1-P1 finds values elevated one to two orders of magnitude higher in the re-entry well. Some portion of this is due to the associated tritium, as it is a beta emitter, though Claassen (1978) identifies some shorter half-lived components (half-lives of 50, 66, and 330 days), based on decay of the activity with time. Claassen estimates an average distribution coefficient, K_d , for the beta/gamma activity of about 2.5×10^4 ml/g, and a time to attain sorption equilibrium of about 500 days. Claassen cautions that extrapolation of the radiochemical data to estimate the radioactive-source water is not possible. As a result, the source term is defined as described in the previous section, using the classified data, rather than estimated from the UA-1-P1 sampling results.

3.1.2 Release Functions

Radionuclides produced by an underground nuclear test are present in three basic forms: gases, surface deposits, and volume deposits (Smith *et al.*, 1995), the proportions of which can change with time after the detonation. Immediately after the detonation, essentially all of the radionuclides are part of a superheated, expanding gas (Borg *et al.*, 1976). When the temperature and pressure start to drop, many of the gases condense. The condensation occurs based on the boiling point of the nuclide, with the higher-boiling points (first to condense) referred to as refractory nuclides, and the lower-boiling point species referred to as volatile. A high percentage of the refractory species is trapped in the solidifying melt, much of which collects at the base of the cavity as “puddle glass.” These are the volume deposits, whose release is controlled by dissolution of this glass.

Nuclides with somewhat lower boiling points (*e.g.*, Cl, I) remain volatile longer and are able to migrate upward through cracks in the rubble chimney. Some portion of these are included within the solidifying puddle glass, but a portion is also deposited as coatings on chimney rubble surfaces. Nuclides included in these surface deposits can be released by relatively rapid processes such as ion exchange, as well as by dissolution, and thus the surface deposits are more susceptible to leaching than the volume-deposited radionuclides. Ion exchange and dissolution of these surface coatings are

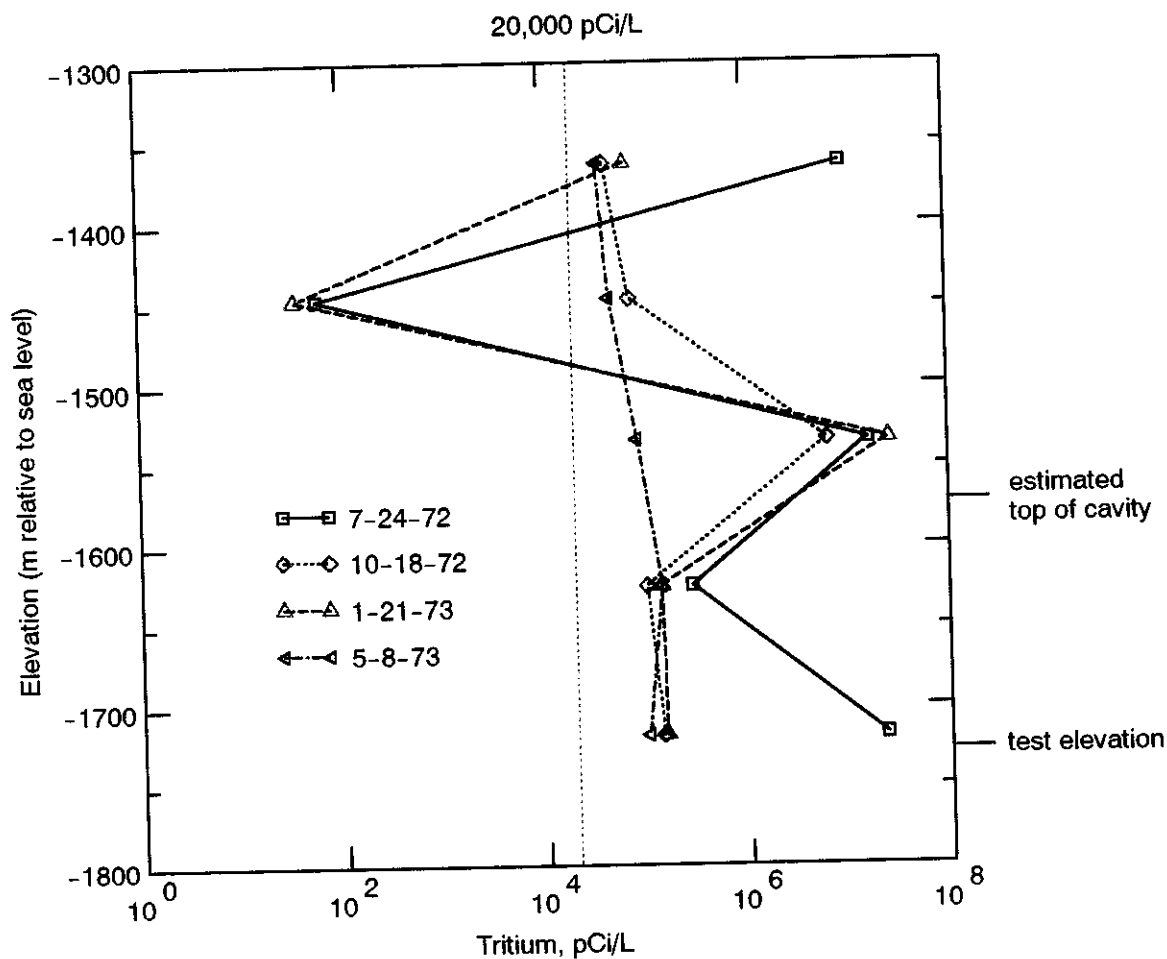


Figure 3.2. Tritium analyses for three sampling events in the Cannikin post-test hole, UA1-P-1. Data from Claassen (1978).

dependent upon the mineralogy of the precipitates and their controlling thermodynamics. The specific form that these surface deposits take at Milrow is unknown, as well as the conditions controlling any dissolution reactions. For these reasons, no attempt is made to formulate a geochemical release function for the surface-deposited radionuclides. Rather, it is assumed that the surface deposits are immediately dissolved upon contact with groundwater and available for migration through the groundwater system. This assumption results in an overestimation of the availability of the surface-deposited radionuclides for transport, as the dissolution and exchange processes described above may be considerably smaller in magnitude and slower in occurrence than modeled. With no geochemical component to the release, the migration from the cavity of the surface-deposited nuclides is governed by the "hydraulic release." The hydraulic release defines the process of re-equilibration of the hydraulic head within the cavity (recovery to static water level from the depressed condition caused by the test), as well as flushing of contaminants from the cavity by the flow-through of groundwater.

Some of the radionuclides produced remain in gaseous form (*e.g.*, Kr and Xe) and may be trapped in solidifying phases or dissolved in groundwater. Other nuclides are gaseous, but then decay to a non-gaseous nuclide. In these cases, the preceding decay-chain behavior is an important control on the distribution and release of daughter nuclides. For example, both ^{137}Cs and ^{90}Sr can be found in surface deposits throughout the chimney, as well as in the puddle glass, because of gaseous precursors. Prompt injection is another release process that may transport gaseous species under early cavity conditions. Gaseous tritium and strontium and cesium precursors may be forced several cavity radii away from the detonation point through explosion-induced fractures arranged radially away from ground zero (Smith, 1995). It is uncertain whether refractory species are transported by prompt injection. At Long Shot, tritium and krypton detected in mud pits and relatively shallow wells are attributed to early-time gas migration upward through the chimney and into the spall zone, where the gas then dissolved in groundwater (Castagnola, 1969). No similar gas migration was detected at Milrow nor Cannikin.

Several of the processes described above require elaboration to understand how they are implemented in the transport analysis. Following are additional discussions of the apportioning of radionuclides between volume and surface deposits, and of the release of radionuclides from the source.

3.1.2.1 Volume/Surface Mode Designation

Refractory and volatile behavior designations are culled from literature references (Borg *et al.*, 1976; Borg, 1975; International Advisory Committee, 1998a; Kersting, 1996; Smith, 1995) whenever possible. For those nuclides with no specific literature reference, volatilities of oxides (Bedford and Jackson, 1965; Krikorian, 1981) and melting point temperatures are used to assign a behavior consistent with the volatilities and melting points of known refractory and volatile nuclides.

A small proportion of nuclear melt glass is not incorporated in the bottom puddle, but is distributed through the collapsing chimney as a result of splashes caused by blocks of rock falling into the puddle, or as fine droplets entrained with escaping cavity gases (Smith, 1995). The exact amount distributed in this way is not known. Based on broad experience at Lawrence Livermore National Laboratory, examining glass samples from underground testing (Borg, 1975) estimates that at most only 2 to 3 percent of refractories are lost from puddle glass. Rabb (1970) found that isotopes other than ^{137}Cs , ^{125}Sb , $^{95}\text{Zr}/^{95}\text{Nb}$, ^{147}Pm , and ^{185}W were 95 percent or more in the glass with the remainder elsewhere for the Pile Driver test. The international working group charged with evaluating the source term for the French underground nuclear tests on Mururoa and Fangataufa estimated a partitioning of 98 percent in melt glass and 2 percent on rubble for plutonium isotopes and other transuranium nuclides, while French studies of the same tests assumed 100 percent in the melt glass (International Advisory Committee, 1998a). Based on these sources, it is assumed here that 5 percent of the total mass of even the refractory species is lost from the puddle glass. Thus, the designated refractory radionuclides have 5 percent of their mass considered surface deposited, with the remaining 95 percent volume deposited (Table 3.2).

The distribution of ^{90}Sr and ^{137}Cs is assigned based on fractionation data compiled by Borg *et al.* (1976). They list the fractionation index for several radionuclides from tests in different rock types. The lowest value measured from deeply buried underground tests (neglecting results from shallowly buried tests in alluvium) for incorporation in the glass is applied to the Amchitka evaluation. Thus, it is assumed that 20 percent of the ^{137}Cs is contained within the puddle glass and 80 percent is surface deposited through the cavity and chimney, and 40 percent of the ^{90}Sr is in the puddle glass and 60 percent is surface deposited. The higher proportion of ^{90}Sr in the glass as compared to ^{137}Cs is consistent with the difference in the half-life of their gaseous precursors. The ^{90}Kr half-life is 33 seconds, whereas the ^{137}Xe half-life is 3.9 minutes, allowing more time for migration of the mass-137 chain to migrate out of the puddle glass.

Table 3.2. Release ratios assigned to source term nuclides.

Element	Hydraulic Release (%)	Volume (Glass) Release (%)
H (Hydrogen)	100	0
C (Carbon)	100	0
Cl (Chlorine)	50	50
Kr (Krypton)	100	0
Sr (Strontium)	60	40
Tc (Technetium)	20	80
I (Iodine)	50	50
Cs (Cesium)	80	20
Sm (Samarium)	5	95
Eu (Europium)	5	95
U (Uranium)	5	95
Np (Neptunium)	5	95
Pu (Plutonium)	5	95
Am (Americium)	5	95

The halogens, ^{36}Cl and ^{129}I , can be expected to have volatile behavior in the early time, but there are also natural analogs in the geologic environment whereby halogens are included in volcanic glass (Hampton and Bailey, 1984). As the steam condenses in the cavity, some of the volatiles will be trapped and incorporated in the glass. It is assumed here that 50 percent of the ^{36}Cl and ^{129}I is included in the glass, and the remaining 50 percent is surface deposited. Technetium-99 (^{99}Tc) is relatively volatile, but has short-lived refractory precursors that are assumed here to trap 80 percent of the mass in the glass (International Advisory Committee, 1998a).

By a similar process, other volatile nuclides are probably entrained in the melt. For example, the French report that more than 50 percent of the available tritium is captured by their glasses (Dupuis, 1970, as reported by Borg, 1975). Borg (1975) reports that only a small (but unquantified) portion of the total tritium produced can be recovered from glasses of tests conducted in saturated alluvium and tuff. At Pile Driver, Borg (1975) estimates that 1.53 gm of a total 1.8 gm produced by activation is contained in the melt, but notes that this is considerably less than the total tritium

available. Given these uncertainties and the importance of tritium to the transport calculations, no incorporation in the melt glass is assumed here. The size of the carbon dioxide molecule can limit its inclusion in volcanic glasses, (though carbon monoxide may dissolve; Hampton and Bailey, 1984), and krypton is noncondensable, so these nuclides are also considered subject only to the hydraulic release function.

3.1.2.2 Release Rate

It is well established that nuclear cavities and chimneys are dewatered and subsequently refilled, though the process through which the dewatering occurs is largely inferred (Borg *et al.*, 1976). Within the cavity itself, the depressed water levels probably result from thermal and compressional forces generated by the nuclear reaction. Following the desaturation immediately after the test, the cavity and chimney will infill with groundwater flowing radially from the surrounding saturated rock. While hydraulic head within the chimney is depressed below that in the surrounding aquifer, there is no hydraulic force to drive contaminant migration. Given this, radionuclides are not expected to exit the cavity and begin transport through the aquifer until after infilling is completed. At some underground nuclear test sites, the infill process has required decades, and this time has been accounted for in radioactive decay of the source (Pohll *et al.*, 1998; Pohlmann *et al.*, 1999). Estimated cavity infill times for Amchitka are relatively short by comparison, predicted to be 500 days for Milrow based on subsurface hydrologic data (USGS, 1970), and 290 days for Cannikin, based on the time of infilling of Cannikin Lake within the collapse sink (Gonzalez, 1977). Given that the impact of decay over a one- to two-year period is insignificant for the half-lives of the radionuclides considered here, transport is conservatively assumed to begin immediately after the detonation date of each test.

The rock, fission products, and device components that are vaporized by the tremendous heat and pressure of a nuclear reaction quickly begin to condense and coalesce into nuclear melt glass. This glass (a solid with no crystalline structure) contains much of the radioactivity produced by a nuclear test. Radionuclides must be removed from the melt glass to be transported by groundwater. Available data for predicting nuclear melt glass dissolution are presented in a transport analysis performed for the Shoal underground nuclear test (Pohll *et al.*, 1998). The approach selected for that site, and also applied here, is to use dissolution rates based on analogy to the dissolution of volcanic glass. This approach avoids the significant problems inherent in trying to use data from nuclear melt glass leaching experiments, such as data collected during nonequilibrium conditions.

Dissolution of glass in contact with groundwater collected from the depth interval of 1,169.8 to 1,230.2 m in well UAe-2 (the device emplacement depth was 1,218 m) is expected based on thermodynamic considerations. The log of the ion activity product to the equilibrium constant ($\log IAP/K_T$) for amorphous silica is -1.62. The silica content of this particular sample is comparatively low, but the next higher sampled interval, at a depth range of 1,057.6 to 1,127.8 m, remains undersaturated with respect to amorphous silica, despite a higher dissolved silica content ($\log IAP/K_T$ of -0.85). The rate equation used to calculate nuclear melt glass dissolution follows a linear rate law (White, 1983):

$$\zeta = \zeta_0 + k_f t \quad (3.15)$$

where ζ is the mass transfer of a chemical species into aqueous solution per unit surface area of solid (moles/cm²), ζ_0 is the mass transfer at zero time, which is a function of initial surface ion exchange (moles/cm²), k_f is the linear rate constant (moles/cm²s), and t is the time(s).

The bulk composition of volcanic glass and analyzed nuclear melt glass is similar (Table 3.3). Though there are no analyses of the bulk elemental composition of Amchitka nuclear melt glass, nuclear melt glass tends to resemble the bulk rock composition because there is no appreciable migration of major elements from a cavity region (Schwartz *et al.*, 1984). Chemical analysis of rocks collected from the working points of Long Shot, Milrow, and Cannikin are 49 to 62 percent SiO₂ and 15 to 16 percent Al₂O₃ (Table 3.3). This composition is closest to that of the trachytic glass used by White (1983) in his dissolution experiments, so that the dissolution constant used here is the one determined from his experiment T-2, at a pH of 6.2, with a k_f of 0.97×10^{-15} moles/cm²s and an initial exchange value, ζ_0 of 0.34×10^{-9} moles/cm².

Table 3.3. Comparison between chemical composition of natural volcanic glass, nuclear melt glass, and bulk rock composition at the Amchitka testing intervals. Major and trace element composition in terms of oxides, given as weight percents.

	SiO ₂	Al ₂ O ₃	FeO	MgO	CaO	Na ₂ O	K ₂ O
Perlite*	74.2	14.1	0.15	0.49	1.0	4.0	4.8
Obsidian*	76.0	13.8	0.40	0.011	0.21	4.4	4.5
Trachytic*	62.8	15.2	1.3	0.38	1.1	8.4	5.1
Nuclear Melt Glass†	73.1 (4.9)	14.2 (2.5)	1.18 (1.59)	0.22 (0.27)	1.06 (0.86)	3.49 (1.68)	6.6 (4.2)
Long Shot, 725m††	53.8	15.8	4.2	4.0	5.4	3.8	2.5
Milrow, 1,221 m††	61.5	15.0	3.5	2.2	1.6	5.7	3.6
Cannikin, 1,785 m††	48.9	14.5	7.5	5.7	8.3	4.3	0.95

*Glassy volcanic rocks, as reported by White (1983)

† Average of six nuclear melt glass samples, as reported by Smith (1995), with standard deviations in parentheses

†† Analyses of rocks from the working points of the respective tests from Gard (1972)

With the dissolution rate constant given on a per unit surface area basis, the specific surface area is a very sensitive term in the dissolution equation. It is also a parameter that is poorly known from experimental work and wholly unknown for in-situ cavity conditions (Pohll *et al.*, 1998). This uncertainty is addressed by considering a distribution of specific surface areas, leading to a distribution of release rates. The mean value used here, 25 cm²/gm, is equivalent to the value leading to the glass release used in the evaluation of the French underground tests on Mururoa and Fangataufa (International Advisory Committee Working Group 4, 1998). This value is between two extremes evaluated elsewhere for specific surface area of nuclear melt glass. Essington and Sharp (1968) measured specific surface area for larger particle sizes of nuclear melt glass collected from

the Rainier test and reported a value of 500 cm²/gm, but concerns have been raised regarding the lower limit of detection of the instrumentation used at that time. This high specific surface area is used to derive the upper bound on the release rate. Recent work evaluating the melt glass produced by the Cambric test (Tompson *et al.*, 1999) applied studies of nuclear waste glass surface area to postulate much lower values of specific surface area (approximately 0.52 cm²/gm). The lower end of the release rate distribution considered here, 4 cm²/gm, is conservatively an order of magnitude higher than the Cambric value. The range evaluated here (4 to 500 cm²/gm) coincides reasonably well with the range of 10 to 100 cm²/gm expected as the recommended range for hydrologic source term modeling in recent research into melt glass surface areas (Bourcier *et al.*, in prep).

The total mass of glass available for dissolution is estimated based on a relationship of 700 metric tons of glass produced per kiloton yield (Smith, 1995), and maximum estimates of 80 kt, 1,000 kt, and 5,000 kt for Long Shot, Milrow, and Cannikin, respectively (U.S. DOE, 2000). The resultant thousands of metric tons of glass are assumed to have a gram formula weight of 60 gm/mole and density of 2.65 gm/cm³. The dissolution is calculated iteratively to account for the continual reduction in dissolution as the total surface area is reduced. At each time step of one year, the amount of dissolution is calculated. That lost mass (mass transferred from glass to solution) is then subtracted from the initial mass of that time step to determine the new (reduced) total mass and related (reduced) specific surface area necessary to determine the amount of mass lost in the next time step. As the mass and surface area get smaller, less dissolution occurs with each time step, with that reduction expressed as an exponential decline. Particles are released into the flow field according to an exponential function to approximate the glass dissolution process (this is elaborated in Section 3.3). The release coefficient, k_g , is the product of the specific surface area, the dissolution rate constant, and the gram formula weight. The derivation of k_g from Equation 3.1 is given in Appendix B. This approach for handling glass dissolution assumes adequate flow of groundwater such that saturation with amorphous silica is not reached in the water. If this assumption is violated, even slower dissolution of the puddle glass than used here would result.

Using the mean k_g value of 2.44×10^{-7} days⁻¹, about 50 percent of the glass in the Milrow cavity is calculated to be dissolved after approximately 15,000 years (Figure 3.3). More mass is dissolved in early time, with a trailing tail in later years. At the upper end of the release rate distribution (specific surface area of 500 cm²/g and k_g of 2.5×10^{-6} day⁻¹), 50 percent of the mass has dissolved after about 600 years, while it requires almost 100,000 years to dissolve half the mass at the lower end of the distribution (specific surface area of 4 cm²/g and k_g of 1.6×10^{-8} day⁻¹). The other extreme value of 0.52 cm²/g ($k_g = 2.6 \times 10^{-9}$ day⁻¹) used by Tompson *et al.* (1999) requires hundreds of thousands of years to dissolve half the mass; only 9 percent is dissolved at 100,000 years. These calculations neglect rate-reducing processes such as protection of the glass from additional dissolution by the formation of a mantle of reaction products.

Nuclear melt glass dissolution for underground tests in the Pacific, including the French tests in the South Pacific and the tests at Amchitka, was examined by Smith and Bourcier (1999). Though they selected a higher rate constant than used here, their estimate of surface area was much smaller (0.07 cm²/g), resulting in an estimate of 6.7×10^6 years to dissolve all the melt glass within

Amchitka. The rate and specific surface area used in the present study result in dissolution of 98 percent of the glass before 100,000 years, for each test (Figure 3.3). For comparison, Smith and Bourcier (1999) estimate a glass dissolution constant of 7.5×10^7 years for Mururoa and Fangataufa, whereas the IAEA use a glass lifetime of 405,000 years.

3.2 Retardation

Radionuclides that are dissolved in groundwater and available for transport are subject to a variety of physical and chemical processes that can retard their movement relative to the movement of water. Together, these processes are referred to as retardation and include ion exchange, adsorption, and surface and bulk precipitation. Sorption and matrix diffusion are powerful retardation mechanisms that need to be incorporated in the transport analysis. The data necessary to consider individual reactions are not available for the Amchitka tests; instead, a bulk sorption approach is used to approximate chemical processes. This approach is limited to equilibrium-controlled processes. Kinetic processes, particularly diffusion, can be important in controlling the rate of other retardation processes and may result in additional significant inhibition of radionuclide transport. The supporting data for sorption, and how it is applied to the modeling, are presented first, followed by a discussion of the treatment of matrix diffusion.

The distribution coefficient, K_d , is a measure of partitioning of an ion between the solution and the solid under equilibrium conditions. Distribution coefficients were presented for a basalt sample

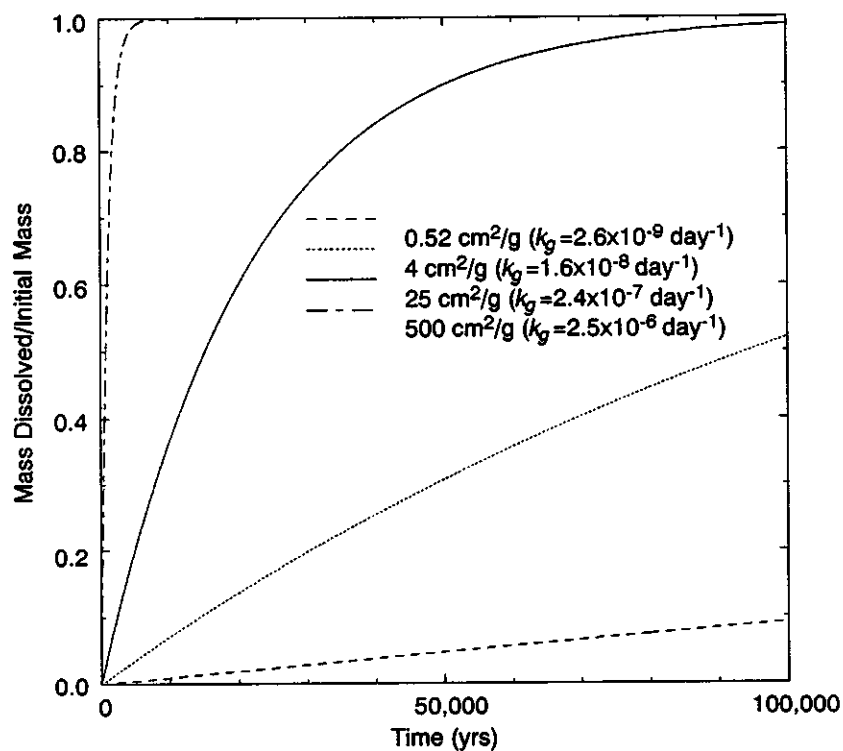


Figure 3.3. Dissolution function for nuclear melt glass, using the parameters described in the text and various values for the specific surface area.

from Amchitka by Nork and Fenske (1970). They report K_d values for Sr ($1.07 \times 10^{-6} \text{ m}^3/\text{gm}$) and Cs ($6.5 \times 10^{-6} \text{ m}^3/\text{gm}$) for the basalt in contact with seawater.

Given the important role such K_d values would play in estimating migration, validation and refinement of the sorptive properties of the aquifer matrices of Amchitka are performed through a new series of experiments. The experiments are conducted using cores from Amchitka drillholes with synthetic groundwater based on chemical analyses of groundwater from well UAe-2 from the interval 1,530 to 1,590 m below land surface. This groundwater is representative of the composition below the transition zone; it is similar to seawater. This is chosen because sorption can be significantly reduced by the competition for reaction sites with higher ionic strength waters, and therefore will result in more conservative (lower) distribution coefficients than experiments with water simulating the freshwater lens. Two aquifer materials are investigated: basalt and breccia. The basalt core is from the Cannikin emplacement well, UA-1, at a depth of 1,819 m. The breccia core is from the same borehole at a depth of 1,885 m.

It is impractical to run individual sorption experiments for all of the elements in the nuclear source term, plus daughter products, especially given the hazardous and controlled nature of many of the elements. Rather, surrogates are identified to approximate the actual source term. Strongly and moderately binding cations (lead and cesium, respectively) are evaluated for their affinity for the different aquifer materials. Previous investigations (Pohll *et al.*, 1998; Pohlmann *et al.*, 1999) also examined anion reactions, but they were found to be relatively insignificant even in freshwater aquifers, so are not included here. Initial work with strontium resulted in dissolution of strontium from the rocks themselves such that it is assumed that no significant sorption would occur and thus no further experiments are performed.

The details of the sorption experiments can be found in Appendix C. In general, the sorptive behavior of the breccia is greater than that of the basalt, consistent with the greater reactive surface area identified in the characterization analyses. Sorption of cesium is essentially non-existent on the basalt material at the high-ionic strength used. Cesium is apparently unable to successfully compete with other cations for exchange sites, consistent with the low sorption reported by Nork and Fenske (1970) for experiments conducted with seawater. Additional scoping experiments at lower ionic strength (0.01 molar NaNO_3 , as opposed to 0.5 molar) confirmed that cesium would sorb under less saline conditions, as would be encountered above the seawater transition zone.

Despite the high ionic strength of the solution, lead is able to sorb onto the aquifer material. The linear and Freundlich isotherm parameters for lead are given in Table 3.4. Non-linearity of the sorption isotherms is not severe, as indicated by the Freundlich parameters, particularly for results in the pH range of most groundwater samples (pH of 7 to 8). Lead sorption is strongly pH dependent, varying by two orders of magnitude across the pH range of 6.0 to 9.0. The values of pH reported for Amchitka groundwater are generally in the range of 6.5 to 9.0 (Beetem *et al.*, 1971). A few groundwater samples have anomalously high pH measurements, suggestive of contamination during cementing operations. A compilation of data from water samples collected from nuclear cavities and near cavities indicates pH values near neutral to slightly basic, consistent with regional groundwater in the testing areas (Smith *et al.*, 1997).

Table 3.4. Linear and Freundlich isotherm parameters for lead sorption. Experimental details and discussion are in Appendix C.

pH	Rock type	K_d (m ³ /gm)	K_f (gm/gm)(gm/m ³) ^{1/n}	1/n
6.0	basalt	2.14 x 10 ⁻⁴	2.60 x 10 ⁻⁴	0.77
	breccia	3.17 x 10 ⁻⁴	3.19 x 10 ⁻⁴	0.67
7.0	basalt	4.92 x 10 ⁻⁴	5.75 x 10 ⁻⁴	0.92
	breccia	5.87 x 10 ⁻⁴	5.25 x 10 ⁻⁴	0.72
8.0	basalt	1.91 x 10 ⁻³	2.28 x 10 ⁻³	1.06
	breccia	1.66 x 10 ⁻³	2.09 x 10 ⁻³	0.96
9.0	basalt	1.59 x 10 ⁻²	8.83 x 10 ⁻²	1.53
	breccia	1.43 x 10 ⁻²	3.28 x 10 ⁻²	1.32

3.2.1 Assignment of Distribution Coefficient

Sorption experiments are only performed for strontium, cesium, and lead. The radionuclide source considered here (Table 3.1) includes many more elements, with the total radionuclide source term even more. Those elements that were not subject to the experiments are assigned K_d values by assuming analogous sorptive behavior to those elements with data. This process requires assumptions regarding the likely chemical forms to be found, and obviously includes substantial uncertainty. The resulting sorption assignments are given in Table 3.5.

Table 3.5. Assignment of sorption behavior to radionuclide source elements.

Element	No Sorption	Strongly Sorbing Cation
H (Hydrogen)	X	
C (CO ₃) (Carbon)	X	
Cl (Chlorine)	X	
Kr (Krypton)	X	
Sr (Strontium)	X	
Tc (Technetium)	X	
I (Iodine)	X	
Cs (Cesium)	X	
Sm (Samarium)		X
Eu (Europium)		X
U (Uranium)		X
Np (Neptunium)		X
Pu (Plutonium)		X
Am (Americium)		X

The laboratory analogue for the strongly sorbing cation is lead. In comparative studies of laboratory sorption data, lead is generally weaker sorbing, often by an order of magnitude, compared to some of the elements assigned here (e.g., U, Pu, Np, Am) (Stenhouse and Pottinger, 1994).

However, it should be noted that uranium, and to a lesser degree neptunium, had lower sorption affinities under some conditions tested for Yucca Mountain (Triay *et al.*, 1997). The more reduced conditions likely in the deep aquifers at Amchitka can be expected to promote stronger sorption affinity as compared to the oxidized unsaturated zone at Yucca Mountain. No sorption is applied for strontium and cesium, based on the laboratory study, nor for hydrogen (tritium), carbon, chlorine, krypton, technetium, or iodine, based on their characteristics and previous studies.

To follow the in-growth of daughters along decay chains, it is necessary in the modeling process to use the same sorption behavior assigned to the parent for the daughter because radioactive decay (and daughter ingrowth) are handled in post-processing (individual radionuclides are not tracked during transport, only six solute classes as discussed in the modeling section). In one case, this causes a retardation assignment that is contrary to the expected behavior: ^{85}Rb would be expected to be strongly sorbing, but instead is modeled with no retardation due to the behavior of its parent, ^{85}Kr . This is a conservative assumption that leads to overestimating the concentrations and fluxes of ^{85}Rb .

3.2.2 Calculation of Retardation Factor

Despite the relatively large porosity indicated for the Amchitka formations from core data, the conceptualization of the aquifer considers the bulk of the flow to be through fractures. The dimensionless retardation factor (R) in cases of fast reversible adsorption with a linear isotherm can be represented for fracture flow conditions by:

$$R = 1 + \frac{K_a}{b} \quad (3.16)$$

where K_a [L] is a surface-based sorption constant ($K_a = K_d/A_{sp}$) and b [L] is the mean fracture half-aperture (Freeze and Cherry, 1979; Moreno *et al.*, 1988; Frick *et al.*, 1991). Equation (3.2) is only valid for fractured materials in which the porosity of the solid mass between fractures is insignificant (Freeze and Cherry, 1979), an assumption that may well be violated based on the porosity measurements for the core.

Estimating a partitioning coefficient from the lead sorption experiments using basalt and breccia as sorbents under pH conditions ranging from 6 to 9, a K_d of $1 \times 10^{-3} \text{ m}^3/\text{gm}$ and an A_{sp} of $2.4024 \text{ m}^2/\text{g}$ are used to calculate a K_a of approximately $4 \times 10^{-4} \text{ m}$. No measurements exist for the fracture half-aperture, b . Scoping transport calculations for the NTS estimated fracture apertures for permeable tuffs to range from 2×10^{-4} to $6 \times 10^{-4} \text{ m}$ (GeoTrans, 1995). Fracture apertures at Yucca Mountain are estimated from 6×10^{-6} to $6.7 \times 10^{-5} \text{ m}$ (Peters *et al.*, 1984). Snow (1968) evaluated igneous and metamorphic rocks to 120 m depth and concluded that openings larger than $4 \times 10^{-5} \text{ m}$ would be unusual. The IAEA used a fracture aperture of $1 \times 10^{-3} \text{ m}$ in the South Pacific work. The same aperture value of $1 \times 10^{-3} \text{ m}$ is used here (half-aperture of $5 \times 10^{-4} \text{ m}$). Using these values yielded a retardation coefficient for strongly sorbing cations (lead) of approximately 1.8.

When retardation occurs within the matrix blocks, it is represented by the following equation (Freeze and Cherry, 1979):

$$R_m = 1 + \frac{\rho_b}{\theta_m} K_d \quad (3.17)$$

where R_m is the dimensionless retardation coefficient in the matrix blocks, K_d [L^3/M] is the distribution coefficient, ρ_b is the bulk density [M/L^3], and θ_m is matrix porosity. A bulk density of 2.3 gm/cm^3 is used, based on 99 measurements on core material from UAe-2, UAe-1, UAe-3, and UAe-6 (Lee, 1969a,b,c,d). This value is representative of the bulk density of the breccia formations; the basalt density is higher (2.5 gm/cm^3) and would lead to a larger retardation value. The porosity used is also based on core measurements, a value of 0.12, the mean of 149 core measurements for the deeper Kirilof Point and Older Breccias formations. Given that the matrix retardation formulation leads to high values of R , a partitioning coefficient half of that used in the fracture retardation is applied here, $5 \times 10^{-4} \text{ m}^3/\text{gm}$, which is still within the range of experimental results. These parameter values lead to an R_m value of approximately 9,000.

3.2.3 Matrix Diffusion

Matrix diffusion is a potentially important mass transfer process by which solutes are removed from high-velocity fracture flowpaths into the surrounding matrix. With the decay of radionuclides, long residence times in the rock matrix actually reduce the mass of contaminant, as well as retard the effective velocity. The numerical approach for simulating matrix diffusion is presented in a later section, while the parameter values are discussed here. The matrix diffusion parameter, κ , used here is defined as

$$\kappa = \frac{\theta_m \sqrt{D_m^* R_m}}{b} \quad (3.18)$$

where D_m^* (L^2/T) is an effective diffusion coefficient in the rock matrix, b (L) is the fracture half-aperture, θ_m (L^3/L^3) is the rock matrix porosity, and R_m is the dimensionless retardation coefficient in the rock matrix. The approach to calculating R_m for sorbing radionuclides is described in the previous section. The approach used for estimating κ is to derive the best estimate based on available information, then consider conservatively lower values to address both data uncertainty as well as model assumptions (such as an infinite matrix, as discussed in the approach section).

Matrix diffusion can be expected to be a significant transport process through the volcanics at Amchitka because the porosity of the matrix blocks is relatively high. Core measurements on 197 samples from Amchitka boreholes have a mean porosity of 0.14 with a standard deviation of 0.07, with the deeper units (Kirilof Point and Older Breccias) having an only slightly lower mean at 0.12.

Effective diffusion coefficients are measured on cores from Amchitka, with the details provided in Appendix C. For the conservative ion, bromide, the measurements range from $1.72 \times 10^{-6} \text{ cm}^2/\text{s}$ to $9.23 \times 10^{-6} \text{ cm}^2/\text{s}$. Diffusion coefficients for basically non-sorbing species in materials from Yucca Mountain and the NTS range from 1.0×10^{-7} to $3.5 \times 10^{-6} \text{ cm}^2/\text{s}$ (Triay *et al.*, 1993; Walter, 1982). These experiments were conducted with fresh surfaces of various volcanic lithologies and involved matrix porosities between 0.06 and 0.4. The recent tracer experiments in the fractured lavas at the

Bullion site on the NTS resulted in estimates of diffusion coefficients of 1.4×10^{-7} to 1.9×10^{-7} cm²/s (IT Corp., 1998). The diffusion of tritiated water through saturated devitrified tuffs is found to be on the order of 10^{-6} cm²/s, while large anions that are excluded from tuff pores due to size and charge still record diffusion coefficients on the order of 10^{-7} cm²/s (Triay *et al.*, 1997). The IAEA, in its evaluation of radionuclide diffusion into volcanics at the South Pacific French underground testing sites, used a diffusion coefficient of 1×10^{-7} cm²/s (IAEA, 1998).

As in the retardation calculation, the fracture half-aperture probably presents the largest uncertainty in the matrix diffusion calculation. Larger fracture apertures are more conservative in the calculation (inhibit matrix diffusion), but are difficult to justify at depths of hundreds of meters due to overburden pressure. A half-aperture of 5×10^{-4} m is used for the diffusion calculations, implying fracture openings of one millimeter at depths in excess of 1,000 m.

Combining the values described above leads to a matrix diffusion parameter, κ , of $1.37 \text{ day}^{-1/2}$ for nonsorbing solutes (θ_m of 0.12, D_m^* of 3.27×10^{-5} m²/day, b of 5×10^{-4} m), and a κ of $130 \text{ day}^{-1/2}$ for strongly sorbing cations (including the R_m of 9,000). The parametric uncertainty analysis of the transport modeling considers a minimum κ of $0.0394 \text{ day}^{-1/2}$, maximum of $1.37 \text{ day}^{-1/2}$, with a mean of $0.352 \text{ day}^{-1/2}$ for nonsorbing solutes. The upper end of this range is equivalent to the best estimate derived above, and the lower end is almost two orders of magnitude lower.

In the main transport modeling stage, κ is not varied and is assigned the value of $0.434 \text{ day}^{-1/2}$ for nonsorbing solutes. This is consistent with the parameters above, except the diffusion coefficient is taken an order of magnitude lower (θ_m of 0.12, D_m^* of 3.28×10^{-6} m²/day, b of 5.0×10^{-4} m). Strongly sorbing cations are assigned a κ value of $41 \text{ day}^{-1/2}$, consistent with an R_m of 9000. As presented later in the report, a sensitivity scenario was evaluated using a κ value for nonsorbing solutes of $0.0434 \text{ day}^{-1/2}$. In this sensitivity analysis, sorbing solutes are also considered (R_m of 9000), using a κ of $4.117 \text{ day}^{-1/2}$.

3.3 Solving the Contaminant Transport Problem

Transport of a nonreactive solute in saturated porous media of constant porosity is described by:

$$\frac{\partial C(X, t)}{\partial t} + \nabla \cdot [C(X, t)V(X)] - \nabla \cdot [D(X) \nabla C(X, t)] = 0 \quad (3.19)$$

where $C(X, t)$ represents concentration, $V(X)$ is the velocity vector at location X and $D(X)$ represents the diagonal of the local hydrodynamic dispersion tensor. The components of $D(X)$ are given as (Bear, 1972)

$$D_{ij} = \delta_{ij} \alpha_T |V| + (\alpha_L - \alpha_T) \frac{V_i V_j}{|V|} + \delta_{ij} D^* \quad (3.20)$$

where δ_{ij} is the Kroneker delta ($\delta_{ij} = 1$ for $i=j$ and $\delta_{ij} = 0$ for $i \neq j$), α_L and α_T are the longitudinal and transverse local dispersivities, $|V|$ is the magnitude of velocity, and D^* is the effective coefficient of molecular diffusion.

Several numerical approaches can be used to solve the transport equation, for example, finite differences, finite elements, method of characteristics, and random walk particle-tracking methods. In this study, the random walk method is used to simulate the transport and evolution of radionuclides in the generated random velocity fields. The injected mass is replaced with a large number of particles NP of equal mass m that are tracked in the space-time domain. The initial mass is assumed to be unity and is represented by 20,000 particles in all the transport simulations.

The positions of the particles are updated at each time step according to the random walk equation (Kinzelbach, 1988; Tompson and Gelhar, 1990)

$$X_{t+\Delta t} = X_t + [V(X_t, t) + \nabla \cdot \mathbf{D}(V(X_t, t))]\Delta t + [2\mathbf{D}(V(X_t, t))\Delta t]^{1/2} \cdot \mathbf{Z} + \frac{D(V(X_t, t))}{\theta} \nabla \theta \quad (3.21)$$

where $X_{t+\Delta t}$ is the updated position of the particle that was at X_t in the previous time step, $V(X_t, t)$ is the velocity vector at the old position at time t , \mathbf{D} is the local-scale dispersion tensor, Δt is the time step, θ is the spatially varying porosity (between cavity/chimney and the surrounding rock), and \mathbf{Z} is a vector of normally distributed random numbers of zero mean and unit variance. The first term on the right-hand side of Equation (3.7) represents the advective step and the second term adds the effect of the gradients of the dispersion tensor on the particle movement. This latter term is important if sharp fronts exist and whenever the gradient of \mathbf{D} is significant. The term involving the porosity gradient accounts for the porosity variability in the modeled domain. The last term represents the contribution of local-scale dispersion and Brownian diffusion to the movement of the particles.

The need for incorporating the gradient terms for the dispersion coefficient and porosity in Equation (3.7) arises due to the spatial variability of the two parameters within the modeled domain. These gradient terms assume that this variability is sufficiently smooth that one can define these gradients at any point in space. However, when abrupt changes occur in space, as is the case here due to the cavity and chimney formation, these gradients cannot be defined at the interfaces between varying blocks. An alternative to computing these gradient terms was recently proposed by La Bolle *et al.* (2000), where they developed a stochastic partial differential equation that is valid for discontinuous properties such as dispersion and porosity. They also integrated these equations with the random walk particle-tracking method, which resulted in an algorithm that avoids the computation of gradient terms. We show in Section 6 the details of this modified approach and compare it to the traditional gradient-based approach (Equation 3.7). It was found that the modified approach, which is believed to be more accurate, leads to lower mass flux compared to using Equation (3.7), and as such we remain conservative and use Equation (3.7) throughout this report.

The output velocity fields of the FEFLOW solution are obtained at an irregular finite element mesh. However, for convenience and simplicity in computations, the velocity values are interpolated on a uniform grid. The particle velocities needed in the above equation are then obtained by using a bilinear interpolation scheme using the velocities at the four grid points surrounding the particle location. The numerical issues and accuracies associated with this interpolation are discussed and evaluated in detail in Section 6.

The nuclides are assumed to all be located within the cavity. In the case of Long Shot, this equates to four grid cells in the cross-sectional model; four at Milrow, and nine at Cannikin. Since the radionuclides are divided among surface deposits that can be released via hydraulic release and volume deposits, which are trapped in a puddle glass, the treatment of particles representing both categories is different. Assume that p is the percentage of mass released hydraulically, and thus $1-p$ represents the mass in the glass. If the total number of particles is NP , then a number of particles equal to $p \times NP$ is released instantaneously (at time 0, which is equivalent to the test date) into the flow field and is subject to all the processes involved (advection, local dispersion, retardation, etc.). Particles in the glass, $(1-p)NP$, are released in patches according to the glass release coefficient, k_g (T^{-1}) (see Appendix B). Therefore, the number of particles released at any time, $t > 0$, is obtained from the expression

$$NP_G^t = [(1-p)NP] * [(1-e^{-k_g t}) - (1-e^{-k_g(t-\Delta t)})] \quad (3.22)$$

where NP_G^t is the number of particles released from the puddle glass at time $t > 0$. At time $t = 0$, no particles are released from glass and only those released via hydraulic equilibrium are allowed to move with the flow field. Figure 3.4 depicts the number of particles released at every time step for a scenario of 95/5 glass/hydraulic release and a total number of particles of 20,000. The value of the glass dissolution rate, k_g , in this figure is $1.17 \times 10^{-7} \text{ day}^{-1}$. The top plot of Figure 3.4 shows that the number of particles released at $t = 0$ (denoted by the square symbol) is 1,000, which represents the hydraulic release ($0.05 \times 20,000$). No particles are released from the puddle glass at this time. After one time step (e.g., 40,000 days), an initial patch of particles is released from the glass and is equivalent to about 860 particles. This number decreases exponentially until all the mass is released. As the time progresses, the glass dissolution decreases and thus the number of particles released to the flow field becomes smaller. The lower plot in Figure 3.4 shows the cumulative sum of the particles released at any time. After about 200 time steps (21,900 years), almost all the particles representing the glass were released. However, the transport simulations in the second modeling stage focus on a time scale of about 2,200 years, which is found to encounter the peak mass flux and concentration for most of the cases considered. This implies that only a very small portion of the mass trapped in puddle glass is released to the system and the rest contributes to the mass flux and concentration values at a much later time. Radioactive decay associated with these long times does not allow for a higher peak flux than what occurs within the first 2,200 years.

Using the particle distribution at every time step, three types of information are obtained. First, the total mass-flux breakthrough, $Q(t)$, is obtained for the control plane, which is taken to be the seafloor described by the bathymetric profile. The total mass crossing that boundary is computed at every time step and then normalized by the initial injected mass, M_0 , to yield the total relative mass flux as a function of time. The second type of information represents the normalized point solute flux crossing the seafloor as a function of location and time, $q(x, t)$. Figure 3.5 shows the conceptualization of the transport scenario and the computation of the total and point mass flux. The particles are released from the cavity by either hydraulic release or glass dissolution. They are subjected to advection, dispersion, retardation, matrix diffusion and radioactive decay. When they

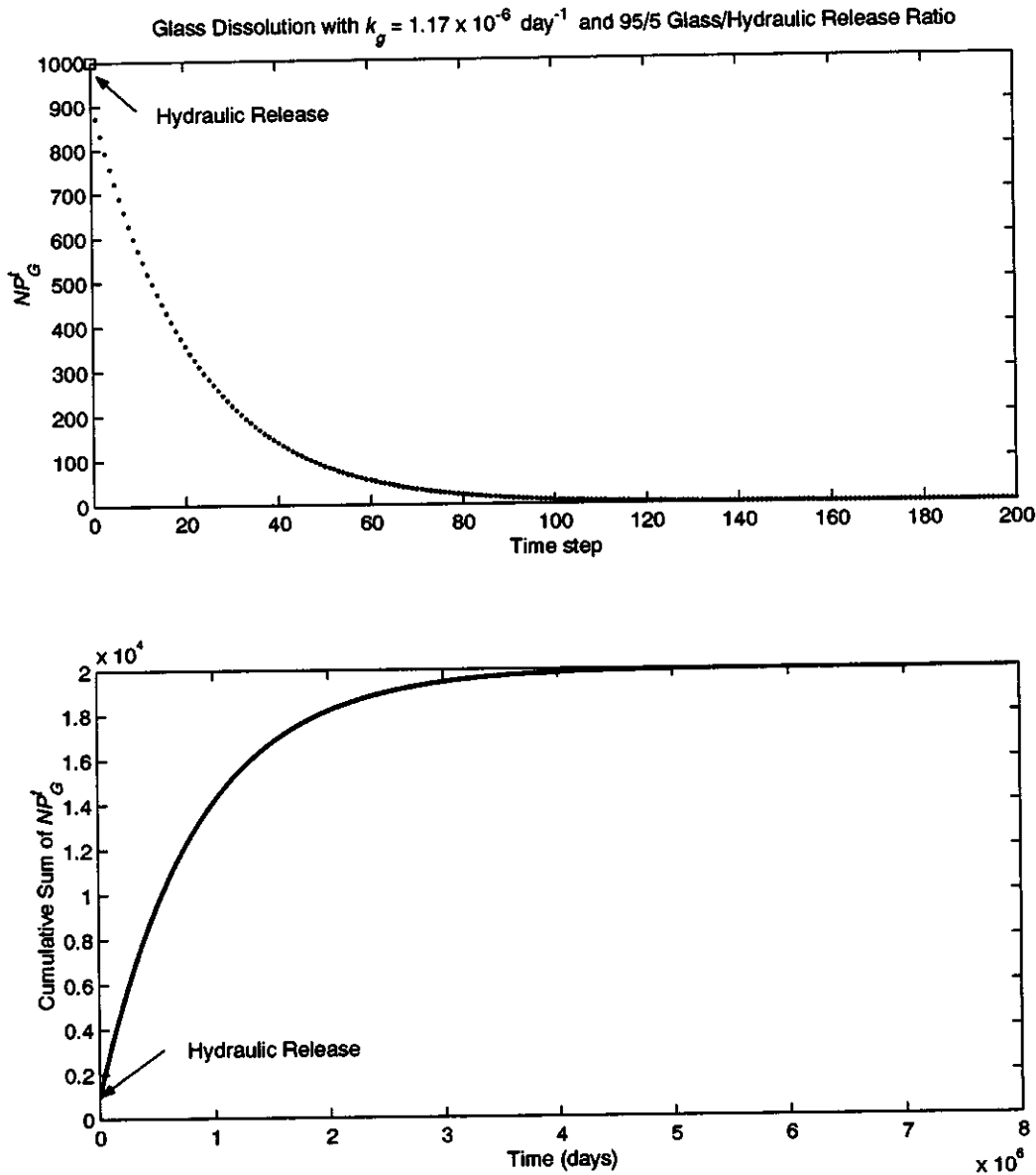


Figure 3.4. Release of particles by glass dissolution rate. The square symbol indicates the number of particles released hydraulically, the top plot indicates the number of particles released at each time step and the bottom plot shows the cumulative sum of the numbers released from time zero to any time t .

reach and break through the seafloor, the point solute flux is computed at segments 40 m in length. Adding all these fluxes at all locations, x , along the bathymetric profile gives the total solute flux as a function of time.

The flux-averaged concentration at these segments is also obtained as a third type of information. One only needs to know the groundwater flux at each of these segments to convert the point mass flux to flux-averaged concentration. The point solute flux is related to the flux-averaged

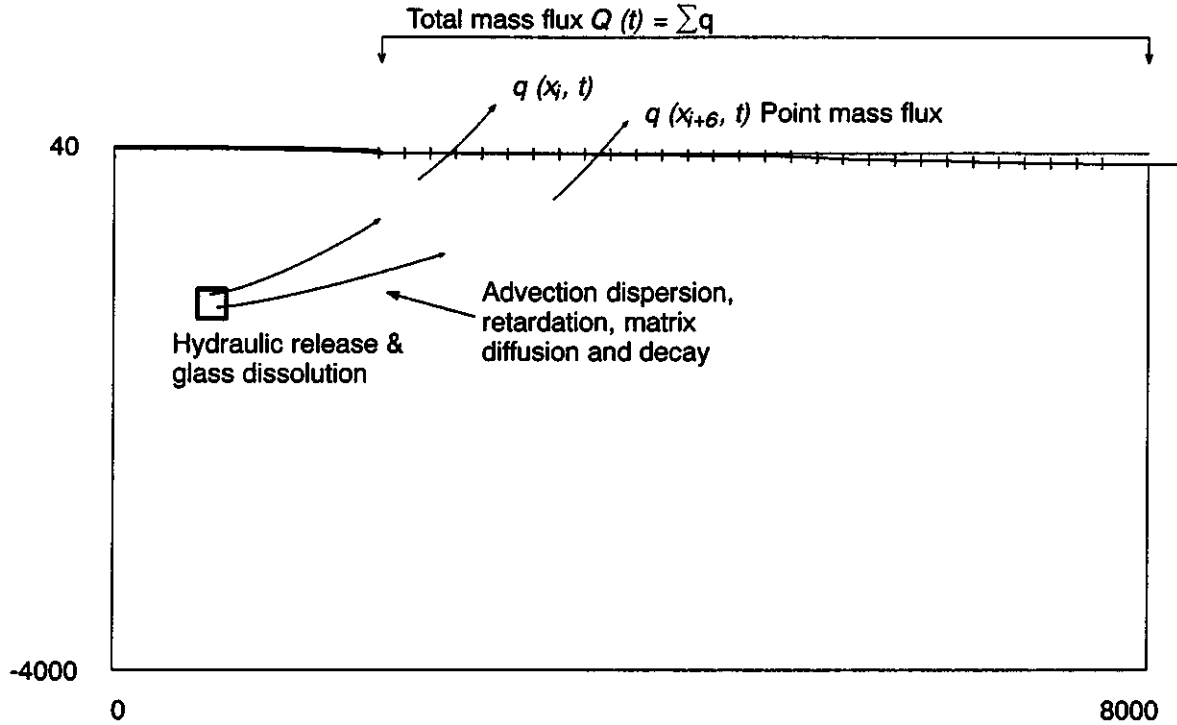


Figure 3.5. Conceptualization of the transport processes and computation of mass flux across the seafloor.

concentration by dividing the former with the groundwater flux (*e.g.*, Kreft and Zuber, 1978; Dagan *et al.*, 1992). The flux-averaged concentration is consistent with common procedures for measuring concentrations in laboratory columns, and in soils, as well as in aquifers (*e.g.*, Kreft and Zuber, 1978; Shapiro and Cvetkovic, 1988). This concentration is then normalized relative to the initial concentration, C_0 . The latter is obtained by dividing the initial unit mass by the water volume within the cavity ($\Delta x_{\text{cavity}} * \Delta y_{\text{cavity}} * 1.0 * 0.07$), where a unit width along the shoreline is assumed and the 0.07 cavity porosity is employed.

For these temporal and spatial-temporal breakthrough results, the outputs are averaged over the ensemble of realizations and statistically analyzed to obtain the mean and the standard deviation. These results are symbolized as $\langle Q(t) \rangle / M_0$, σ_Q / M_0 for the total solute flux, $\langle q(x,t) \rangle / M_0$, σ_q / M_0 for the point solute flux, and $\langle C(x,t) \rangle / C_0$, σ_C / C_0 for the flux-averaged concentration. These undecayed moments will be the same for all nuclides in a given solute class that represents a particular combination of hydraulic/geochemical release ratios and retardation factors. The moments are subsequently decayed for individual nuclides based on their half-lives using the formula

$$[\mu_d(t)]_i = [\mu(t)] e^{-(\ln 2) t / \omega_i} \quad (3.23)$$

where $[\mu_d(t)]_i$ is the decayed moment (mean or standard deviation) for nuclide i at time t , $[\mu(t)]$ is the undecayed moment for the scenario to which nuclide i belongs, ω_i is the half-life of nuclide i in days, and t is the time at which moment is computed in days.

For the general case of the decay of a parent isotope (N_1) to a radioactive daughter (N_2), which decays to a second daughter (N_3) through the final daughter (N_n), $N_1 \rightarrow N_2 \rightarrow N_3 \dots N_n$, the solution giving the number of atoms of any member of the decay series as a function of time and assuming zero initial mass for the daughters ($N_2^0=N_3^0=\dots N_n^0=0$) has the form (Faure, 1977):

$$N_n = \epsilon_1 e^{-\lambda_1 t} + \epsilon_2 e^{-\lambda_2 t} \dots + \epsilon_n e^{-\lambda_n t} \quad (3.24)$$

where the coefficients (ϵ_n) are defined as:

$$\epsilon_1 = \frac{\lambda_1 \lambda_2 \dots \lambda_{n-1} N_1^0}{(\lambda_2 - \lambda_1)(\lambda_3 - \lambda_1) \dots (\lambda_n - \lambda_1)} \quad (3.25)$$

$$\epsilon_2 = \frac{\lambda_1 \lambda_2 \dots \lambda_{n-1} N_1^0}{(\lambda_1 - \lambda_2)(\lambda_3 - \lambda_2) \dots (\lambda_n - \lambda_2)} \quad (3.26)$$

and λ_n is the decay rate for radionuclide N_n . In a case where the initial mass of the daughter radionuclide is not zero (*i.e.*, the radionuclide is also present in the original source), the source mass and the daughter's mass are calculated separately and summed afterward.

The above description of transport modeling applies for the porous medium approach. As discussed earlier in Section 2.1.7, the flow system is conceptualized as a fracture flow system with high velocity in the fractures that separate adjacent porous blocks. The approach we employ is a continuum approach in the sense that discrete fractures are not considered in space, but instead, effective fracture properties (high conductivity and low porosity) are assigned to the discretized domain blocks. Therefore, particles are tracked in space in the same manner as for a porous medium, but they experience the very high fracture velocity within each block. Therefore, for the analysis of transport in a fractured system, the same undecayed moments (mass flux and concentration mean and standard deviation) are obtained. However, before applying the decay analysis to these moments, matrix diffusion is accounted for using the solute flux analytical solution presented by Cvetkovic and Dagan (1994) and Cvetkovic *et al.* (1999). The breakthrough curves for total mass flux with matrix-diffusion effect can be obtained from

$$Q_{md}(t) = \int_0^{\infty} \gamma(t, \tau) Q(\tau) d\tau \quad (3.27)$$

where $Q(\tau)$ is the undecayed mass flux at time τ , $Q_{md}(t)$ is the mass flux after accounting for matrix diffusion, and $\gamma(t, \tau)$ is the retention function that incorporates the effect of mass transfer between the fracture and the rock matrix. This retention function is given as (Cvetkovic and Dagan, 1994; Cvetkovic *et al.*, 1999)

$$\gamma(t, \tau) = H(t - \tau) \frac{\kappa \tau}{2 \sqrt{\pi} (t - \tau)^{3/2}} e^{-\frac{(\kappa \tau)^2}{4(t - \tau)}} \quad (3.28)$$

where H is the dimensionless Heaviside function, τ is the particle travel time (days), t is the time (days) at which the flux is obtained after accounting for matrix diffusion, and κ is the matrix

diffusion parameter (days^{-1/2}) defined as $\kappa = \frac{\theta_m \sqrt{D_m^* R_m}}{b}$. Here θ_m is the matrix porosity, b is the effective half aperture (m), D_m^* is the effective diffusion coefficient in the rock matrix (m²/day) and R_m is the dimensionless retardation coefficient in the rock matrix. The main assumptions underlying the derivation of the above analytical retention function are a constant aperture along the streamtube, diffusion only perpendicular to the fracture plane, well-mixed conditions over the cross-sectional area of the fracture, and homogeneous, infinite rock matrix with no advection. The radioactive decay can also be incorporated in the retention function. To do so, an additional term, $\exp(-t \ln 2/\omega)$ should be multiplied by the right-hand side of the γ expression, with ω being the half-life.

In summary, a non-decayed breakthrough curve is obtained by the random walk particle tracking method and then convoluted with a retention function that accounts for matrix diffusion (e.g., Cvetkovic and Dagan, 1994; Cvetkovic *et al.*, 1999). This approach treats the fractured system as a stochastic continuum. The retention function, however, is derived for discrete fractures. There is, therefore, some inconsistency in this analysis as the discrete and continuum approaches are mixed. However, this is not unreasonable and it has been used in many European studies dealing with safety analysis and risk assessment (e.g., NAGRA, 1994; Cvetkovic, personal communication).

A crucial assumption underlying this analysis relates to the availability of the rock matrix and the rate of diffusion from the fractures into the rock matrix. It is usually assumed that the rock matrix availability for diffusion is unlimited and that the diffusion rate is constant at all times. In other words, the semi-analytical solution employed here does not allow for rock saturation and ceasing of matrix diffusion. The matrix diffusion continues for as long as there are contaminants moving through the fractures. That may not be true for the actual field situation. Depending on the intensity of fractures, the rock matrix may have a limited capacity to absorb contaminants from the fractures and may reach a level of saturation that prevents any further diffusion into it. There is, therefore, the concern that the transport predictions may overestimate the diffusion into the matrix and thus give lower fluxes and concentrations than what might be the case in the field. Three factors alleviate this concern. First, the matrix diffusion values used to produce the transport results are at least one order of magnitude lower than the best estimate. Secondly, radioactive decay will remove mass from the matrix blocks, particularly for shorter-lived nuclides. Thirdly, the conceptualization of fracture flow at depths exceeding 1,000 m below ground surface may represent an overestimation of the flow velocities at that depth. Fractures tend to close up at large depths due to the overburden pressure and this then may change the flow system from a fractured to a continuum porous medium. For porous medium flow with a porosity three orders of magnitude larger than the fracture porosity, residence times become very long and radioactive decay inhibits breakthrough of most radionuclides with short and moderate half-lives.